JOURNAL OF GUIDANCE, CONTROL, AND DYNAMICS
Vol. 18, No. 4, July–August 1995

Failure Diagnosis System Using ARTMAP Neural Networks

Ren Da* and Ching-Fang Lin†
American GNC Corporation, Chatsworth, California 91311

A novel scheme for diagnosing failures in dynamic systems is presented. After a failure is detected by the state chi-square test, two ARTMAP neural networks are applied to recognize patterns formed by data of the state chi-square test in order to determine when the failure happened, how serious the failure is, and where the failure is located. The efficacy of the proposed scheme is demonstrated by simulation examples where soft failures in an integrated global positioning system/inertial navigation system are successfully diagnosed. An effective approach is also developed to overcome the difficulty of distinguishing gyro failures from accelerometer failures.

I. Introduction

TO maintain a high level of performance in a dynamic control system, it is necessary that failures be detected and isolated promptly, so that appropriate remedies can be timely applied. Although catastrophic or hard failures can be uncovered rapidly by on-line built-in testing (BIT), more subtle or soft failures can only be detected and isolated with recourse to more sophisticated techniques based on error estimation/decision theory.[1–8] The chi-square test is a statistical hypothesis testing method for examining whether a random vector has an assumed mean and covariance. An interesting application of the chi-square test for failure detection was proposed by Brumback and Srinath,[9] where a state propagator was used to provide a failure detection reference (an idea originally due to Kerr[10]), and the chi-square test was used to test the consistency of state estimates of the Kalman filter and the state propagator. The approach is named the state chi-square test (SCST) in Ref. 11 because the chi-square test is applied to monitor the state estimate, rather than the residual, of the Kalman filter.

Two approaches were proposed in Refs. 11 and 12 to improve the performance of the SCST. The first approach is to use a pair of state propagators which are reset alternatively with the data of the Kalman filter to increase their accuracy and thereby enhance detection sensitivity of the system. By cooperative operation of the propagators, a highly accurate and reliable detection reference is obtained. The second approach is to test the state estimates of the Kalman filter individually. Then the information from the state estimates which are most seriously affected by failures is utilized to enhance the detection sensitivity of the SCST.

Failure diagnosis in dynamic systems is also of great importance for practical applications. After a failure is detected, it is highly desirable to know when the failure happened, where the failure is located, and how serious the failure is. Obviously, different failures from different sensors have different effects on system measurements, depending on the relationships between the sensor errors and the system measurements. Since these relationships are carefully considered in the model of the Kalman filter, the state estimates which are directly related to a failure will change much more than those which are less or not related to the failure. Therefore, when the SCST is performed to monitor the estimates of the Kalman filter individually, the patterns formed by the SCST data provide good clues for failure diagnosis.

Neural networks have been shown to be very successful in pattern classification.[13–16] Carpenter et al.[17] derived and analyzed a supervised neural network architecture, called ARTMAP, which has two adaptive resonance theory (ART) modules linked by an inter-ART module. The ARTMAP networks can autonomously learn to classify arbitrarily complex binary input patterns into recognition categories, forming a map from n-dimensional binary vectors into m-dimensional binary vectors. The ARTMAP network was reported to be highly superior to the popular back-propagation neural network in both learning speed and performance.[17] In this paper, the classification ability of the ARTMAP neural network will be applied to diagnosing failures by mapping patterns of the SCST results into patterns describing locations, occurrence time, and seriousnesses of failures.

For failure diagnosis of an integrated global positioning system/inertial navigation system (GPS/INS), another problem encountered is how to distinguish gyro failures from accelerometer failures. Because of poor observability, a gyro failure may result in residual changes which are very similar to changes resulting from an accelerometer failure and vice versa. Therefore, when a failure happens in the x accelerometer (or in the y gyro), the Kalman filter will update the state estimates of both the x-accelerometer error and the y-gyro error at the same time. Consequently, the SCST results related to both of the state estimates may flag the failure. In such cases, failures cannot be simply isolated based solely on the SCST results and, therefore, a specific approach is needed.

Section II describes the working principle of the SCST. Section III presents a structure for failure diagnosis of dynamic systems based on the ARTMAP neural network. The efficacy of the failure diagnosis scheme is shown in Sec. IV when applied to an integrated GPS/INS navigation system. An approach for isolating gyro failures from accelerometer failures is developed in Sec. V. A summary is offered in Sec. VI.

II. State Chi-Square Test

Consider the following error model for a discrete-time dynamic system:

$$\boldsymbol{x}(k+1) = \Phi(k)\boldsymbol{x}(k) + \boldsymbol{c}(k) + \Gamma(k)\boldsymbol{w}(k) \tag{1}$$

$$\boldsymbol{y}(k) = H(k)\boldsymbol{x}(k) + \boldsymbol{d}(k) + \boldsymbol{v}(k) \tag{2}$$

$$E[\boldsymbol{w}(k)] = 0 \qquad E[\boldsymbol{w}(k)\boldsymbol{w}(j)] = Q(k)\delta_{kj} \tag{3}$$

$$E[\boldsymbol{v}(k)] = 0 \qquad E[\boldsymbol{v}(k)\boldsymbol{v}(j)] = R(k)\delta_{kj} \tag{4}$$

where $\boldsymbol{x}(k)$ is an n-dimensional state vector, with Gaussian initial condition $\boldsymbol{x}(0)$, which has a mean $\boldsymbol{x}_0$ and a covariance P_0. The Kronecker delta δ_{ij} is 1, when $i = j$ and 0 otherwise. Vectors $\boldsymbol{x}(0)$, $\boldsymbol{w}(k)$, and $\boldsymbol{v}(k)$ are assumed to be statistically independent. $Q(k)$ is positive semidefinite, and $R(k)$ is positive definite. Vectors $\boldsymbol{c}(k)$ and $\boldsymbol{d}(k)$ represent unknown failures.

If no failure occurs [$\boldsymbol{c}(k) \equiv 0$ and $\boldsymbol{d}(k) \equiv 0$], the following standard Kalman filter algorithm gives the optimal estimate $\hat{\boldsymbol{x}}_K(k \mid k)$ of the system state $\boldsymbol{x}(k)$ (the subscript K identifies terms in the Kalman filter):

$$\hat{\boldsymbol{x}}_K(k+1 \mid k) = \Phi(k)\hat{\boldsymbol{x}}_K(k \mid k) \tag{5}$$

$$P_K(k+1 \mid k) = \Phi(k)P_K(k \mid k)\Phi^T(k) + \Gamma(k)Q(k)\Gamma^T(k) \tag{6}$$

Received May 10, 1994; revision received Dec. 6, 1994; accepted for publication Dec. 12, 1994.

*Principal Scientist. Member AIAA.
†President. Associate Fellow AIAA.

$$\hat{x}_K(k+1\,|\,k+1) = \hat{x}_K(k+1\,|\,k) + K(k+1)\gamma(k+1) \quad (7)$$

$$\gamma(k+1) = y(k+1) - H(k+1)\hat{x}_K(k+1\,|\,\bar{k}) \quad (8)$$

$$U(k+1) = H(k+1)P_K(k+1)H^T(k+1) + R(k+1) \quad (9)$$

$$K(k+1) = P_K(k+1)H^T(k+1)U^{-1}(k+1) \quad (10)$$

$$P_K(k+1\,|\,k+1) = [I - K(k+1)H(k+1)]P_K(k+1\,|\,k) \times [I - K(k+1)H(k+1)]^T + K(k+1)R(k+1)K^T(k+1) \quad (11)$$

with the initial conditions

$$\hat{x}_K(0\,|\,0) = x_0 \qquad P_K(0\,|\,0) = P_0 \quad (12)$$

The SCST detects system failures by monitoring the state estimate of the Kalman filter with the application of the chi-square test. In the SCST, a state propagator is used as a reference system (see Fig. 1), whose state estimate $\hat{x}_S(k)$ and covariance matrix $P_S(k)$ (the subscript S identifies terms in the state propagator) are propagated on the sole basis of the a priori system model information[10]:

$$\hat{x}_S(k+1) = \Phi(k)\hat{x}_S(k) \quad (13)$$

$$P_S(k+1) = \Phi(k)P_S(k)\Phi^T(k) + \Gamma(k)Q(k)\Gamma^T(k) \quad (14)$$

with the initial conditions

$$\hat{x}_S(0) = x_0 \qquad P_S(0) = P_0 \quad (15)$$

Under the conditions

$$\hat{x}_K(0\,|\,0) = \hat{x}_S(0) = x_0 \quad (16)$$

$$P_K(0\,|\,0) = P_S(0) = P_0 \quad (17)$$

the difference between the two estimates

$$b(k) \triangleq \hat{x}_K(k) - \hat{x}_S(k\,|\,k) \quad (18)$$

is a Gaussian random vector with zero mean and covariance $B(k)$, e.g., $b(k) \sim N[0, B(k)]$, where[9]

$$B(k) \triangleq E[b(k)b^T(k)] = P_S(k) - P_K(k\,|\,k) \quad (19)$$

and, thus,

$$\zeta(k) \triangleq b^T(k)B^{-1}(k)b(k) \quad (20)$$

is a chi-square random variable with n degrees of freedom (n is the dimensionality of b), e.g., $\zeta(k) \sim \chi^2(n)$. Then the following detection rule can be considered:

$$\begin{aligned} &\text{if} \quad \lambda(k) \geq 1 \quad \text{then there is a failure} \\ &\text{if} \quad \lambda(k) < 1 \quad \text{then there is no failure} \end{aligned} \quad (21)$$

where $\lambda(k) \triangleq \zeta(k)/\epsilon$, and ϵ is a chosen decision threshold. With the aid of a chi-square distribution table (Mendenhall and Sincich, 1992), the probability of false alarm can be calculated as a function of the window length N and the decision thresholds ϵ.

Two approaches were proposed by Da and Lin[12] to enhance the performance of the SCST.

1) Use a pair of state propagators which are reset alternatively with the Kalman filter data to increase their accuracy and, thereby, the detection sensitivity of the system. Assume t_j ($j = 1, \ldots$) are time points at which one of the state propagators is reset with the Kalman filter data. Then one of the propagators will be reset at $k = t_{2i}$ ($i = 1, \ldots$) and serves as failure detection reference when $t_{2i-1} \leq k < t_{2i}$, whereas the other propagator will be reset at $k = t_{2i-1}$ and serves as the failure detection reference when $t_{2i} \leq k < t_{2i+1}$. By choosing a suitable time interval $\Delta t = t_{j+1} - t_j$, a reliable and highly accurate failure detection reference is obtained.

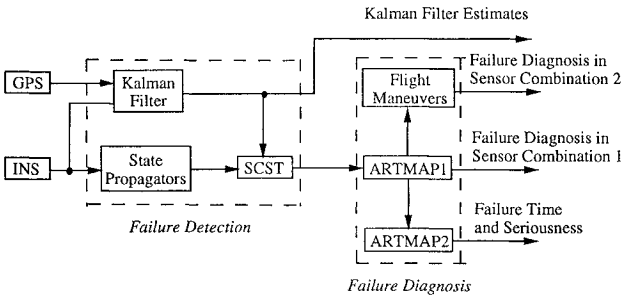

Fig. 1 Failure diagnosis structure for GPS/INS.

2) Test components of $b(k)$ individually. Because $b_i(k) \sim N[0, B_{i,i}(k)]$, where $b_i(k)$ is the ith component of $b(k)$ and $B_{i,i}(k)$ the ith diagonal element of covariance matrix $B(k)$, we have

$$\zeta_i \triangleq b_i^2(k)/B_{i,i}(k) \sim \chi^2(1) \quad (22)$$

Therefore, the components of $b(k)$ can be tested individually with the following detection rule:

$$\begin{aligned} &\text{if} \quad \lambda_i(k) \geq 1 \quad \text{then there is a failure} \\ &\text{if} \quad \lambda_i(k) < 1 \quad \text{then there is no failure} \end{aligned} \quad (23)$$

where $\lambda_i(k) \triangleq \zeta_i(k)/\epsilon_i$, and ϵ_i are the chosen decision thresholds. With this detection rule, the test statistics which are most seriously affected by a failure will detect the failure first. When necessary, the approach can be extended to collectively test two or more closely related components of $b(k)$.

III. Failure Diagnosis Structure

After a failure is detected, it is highly desirable to know when the failure happened, where the failure is located, and how serious the failure is. A failure diagnosis structure for such a purpose in an integrated GPS/INS is shown in Fig. 1 which includes three parts:

1) ARTMAP1 is an ARTMAP neural network[17] which forms a map from patterns of SCST results from sensor errors, at the moment when a failure is detected, into patterns describing locations of different failures.

2) ARTMAP2 is another ARTMAP neural network which associates patterns of SCST results, sampled between $k_b - L + 1$ and k_b, with patterns describing when failures happened and how serious they are, where L is the sampling window width, and k_b is the time the failure is detected.

3) Flight maneuvers are specially designed maneuvers for determining a specific failure for ambiguous cases when the ARTMAP1 cannot identify the specific failure. This kind of situation exists because of poor observability of the GPS/INS systems. This part will be discussed in Sec.V.

A. ARTMAP Neural Network

Developed by Carpenter et al.,[17] ARTMAP is a kind of supervised neural network architecture capable of forming a map from n-dimensional binary vectors into m-dimensional binary vectors by learning examples from the correlated vector pairs $\{a^p, b^p\}$ [dim $(a^p) = n$, dim $(b^p) = m$, and $p = 1, \ldots$]. The ARTMAP neural networks are built up from two fast-learning ART1 modules, called ARTa and ARTb, which are linked by an inter-ART module. Based on the adaptive resonance theory,[13,19] ART1 is itself a class of neural networks capable of self-organizing stable recognition categories for arbitrary temporal sequences of binary input patterns.

The ARTMAP networks need to be trained before being applied to on-line failure diagnosis. On each training trial, an input pattern a^p, presented to the ARTa, is associated with an input pattern b^p, presented to the ARTb, by adjusting the internal parameters of the ARTMAP network, where b^p is the correct prediction given pattern a^p. The system performance can be evaluated by presenting new input patterns, which have never been experienced before, to the ARTa, and then comparing the predicted output patterns in the ARTb with the correct answers. Full definitions and analyses of the ARTMAP networks and ART1 modules are available in the references.[13,17]

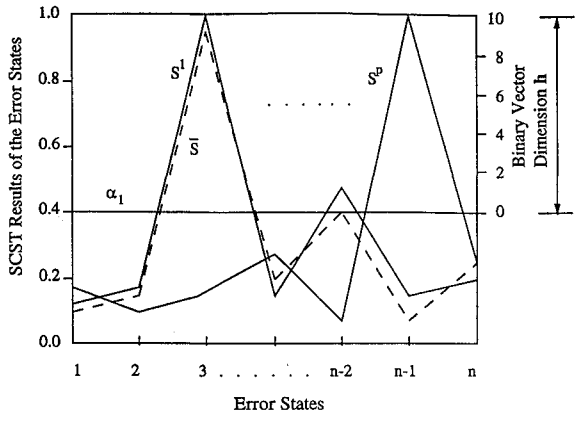

Fig. 2 Illustration of the input pattern organization for the ARTMAP1.

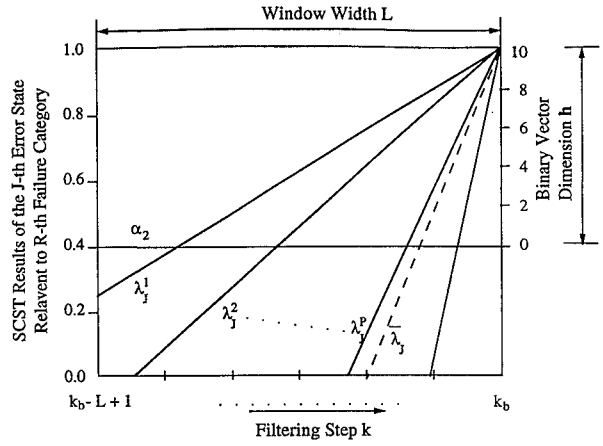

Fig. 3 Input pattern organization for the ARTMAP2.

B. ARTMAP1 Neural Network

Since different failures from different sensors have different effects on the state estimates of the Kalman filter, a good possibility to locate a failure is provided by analyzing the patterns formed by the SCST results at the time step k_b when the failure is detected. This task is carried out by the ARTMAP1 network. Before on-line application, the ARTMAP1 is trained based on a training database, which consists of failure locations and relevant SCST results generated by simulations where different failures in different sensors are assumed. Gaussian process and measurement noise are not added in building the training database, since they do not contain failure features. During training trials, the ARTMAP1 gradually builds up a map from patterns of the SCST results, which are generated from different assumed failures, into patterns describing the locations of these failures.

An illustration of the working principle of the ARTMAP1 is given in Fig. 2, in which the solid lines, denoted by s^p $(p = 1, \ldots,)$, represent patterns of the SCST results from the training database

$$s^p = \left[\lambda_1^p(k_b), \ldots, \lambda_n^p(k_b)\right] \tag{24}$$

where $\lambda_i^p(k_b)$ $(i = 1, \ldots, n)$ is the SCST results of the ith state estimate at time step k_b. [Although the input patterns for the ARTMAP1 (Fig. 2) are discrete, we purposely link them for a better view.] The dashed line, denoted by $\bar{s}$, represents a pattern of SCST results from the on-line failure diagnosis. Then $\bar{s}$ will be classified by the ARTMAP1 into one of its failure categories, denoted by R, such that

$$|s^R - \bar{s}| = \min_p\{|s^p - \bar{s}|\} \tag{25}$$

With this method, the specific failure is identified. The performance of the ARTMAP1 is evaluated on the basis of a testing database formed by simulations where different failures for different sensors are assumed with Gaussian process and measurement noise being considered.

C. ARTMAP2 Neural Network

Evidently, the time when a failure happens is also the time when the SCST statistics begin to change. Serious failures always result in significant changes. Therefore, it is possible to determine when a failure happens and how serious the failure is by means of analyzing the time history of the SCST results. This task is performed by the neural network ARTMAP2. Assume that the ARTMAP1 classifies a failure into a failure category R [see Eq. (25)], the task of the ARTMAP2 is to analyze the SCST pattern of the state estimate J, which corresponds to the failure category R. Figure 3 shows the approach for organizing input data for the ARTMAP2. The k_b used in Fig. 3 represents actually the moments when failures with different magnitudes are detected. At these moments, the calculated test statistic $\lambda = 1$. The lines in the figure show the patterns given by the data sampled from time step $k_b - L + 1$ to k_b. For example, assume $L = 10$, and a failure is detected at $k_b = 100$, e.g., $\lambda_J = 100$. Then the pattern formed by the data will be used for training the ARTMAP2. Also, a training database for the ARTMAP2 can be built by simulations. After training, each of the output neurons of the ARTMAP2 will represent a failure category. It should be noticed that the ARTMAP2's failure category is different from that of the ARTMAP1, because the latter defines the location of a failure, whereas the former specifies the time and seriousness of the failure.

Let the solid lines λ_J^q $(q = 1, \ldots)$ in Fig. 3, for example, represent the SCST patterns formed by failures located in a same place but with different happening time and seriousness. These patterns build a training database for the specific represented by category J. Assume a failure is classified by the ARTMAP1 into its category J, and the dashed line $\tilde{\lambda}_J$ represent the SCST pattern from the on-line failure diagnosis. Then, $\tilde{\lambda}_J$ will be classified by the ARTMAP2 into one of its learned failure categories, denoted by P, such that

$$\sum_{k=k_b-L+1}^{k_b} \left|\lambda_J^p(k) - \tilde{\lambda}_J(k)\right| = \min_p \left\{ \sum_{k=k_b-L+1}^{k_b} \left|\lambda_J^p(k) - \tilde{\lambda}_J(k)\right| \right\} \tag{26}$$

The performance of the trained ARTMAP2 can also be evaluated based on a test database formed by simulations where different failures in different sensors are assumed with Gaussian process and measurement noise being added.

D. Input Pattern Organization

As is well known, organization of input patterns is one of the key factors in practical applications of neural network techniques. Two important issues need to be considered in our case: the choice of the sampling window width L and the method of converting SCST results to a form which can be used to train the neural netwrok. Evidently, the window width influences the neural network performance. Whereas a too large window width results in unnecessarily large dimensionality of the neural network, a too small window width may result in the neural network not having enough information to appropriately diagnose failures. Considering that the learning algorithm of the ARTMAP network is much faster than most of popular supervised networks, such as back-propagation neural networks, the window width can be chosen conservatively.

Since the ARTMAP requires a binary input vector, input pattern $\boldsymbol{a}_{\text{ARTMAP1}}$ for ARTMAP1 should be organized using a coding scheme, called the thermometer code:

$$\boldsymbol{a}_{\text{ARTMAP1}} = [\boldsymbol{a}_{\lambda_1}(k_b), \ldots, \boldsymbol{a}_{\lambda_n}(k_b)] \tag{27}$$

with

$$\boldsymbol{a}_{\lambda_i} = [\underbrace{1 \ldots 1}_{h_i}\ \underbrace{0 \ldots 0}_{(h-h_i)}] \qquad (i = 1, \ldots, n) \tag{28}$$

where h is a chosen integer parameter. As an example, if $h_i = 4$, $h = 6$, then $\boldsymbol{a}_{\lambda_i} = [1\ 1\ 1\ 1\ 0\ 0]$.

As a ramp-type integer function of $\lambda_i(k_b)$, h_i can be calculated by

$$h_i = \begin{cases} h & \text{if} \quad \lambda_i > 1 \\ h * \text{int}[\lambda_i(k_b) - \alpha_1] & \text{if} \quad \alpha_1 \le \lambda_i \le 1 \\ 0 & \text{if} \quad \lambda_i < \alpha_1 \end{cases} \tag{29}$$

where int[x] is an operator which rounds element x to the nearest integer $\le x$. A parameter α_1 where $0 < \alpha_1 < 1$ is chosen, which can be adjusted for reducing the noise influence on the diagnosis system performance (Fig. 2).

An input pattern $\mathbf{a}_{\text{ARTMAP2}}$ for ARTMAP2 is organized as follows:

$$\boldsymbol{a}_{\text{ARTMAP2}} = [\boldsymbol{a}_{\lambda_J}(k_b - L + 1), \ldots, \boldsymbol{a}_{\lambda_J}(k_b)] \tag{30}$$

where $\boldsymbol{a}_{\lambda_J}(k)$ $(k = k_b - L + 1, \ldots, k_b)$ are binary vectors converted from $\lambda_J(k)$ using the same method as that described in Eqs. (28) and (29), where the index J comes from the ARTMAP1.

IV. Failure Diagnosis Simulations

In this section, the proposed ARTMAP networks are applied to the failure diagnosis of an integrated GPS/INS. The chosen error states of the GPS/INS are as follows:

$$\boldsymbol{x}(t) = [\delta r_N, \delta r_E, \delta r_D, \delta v_N, \delta v_E, \delta v_D, \phi_N, \phi_E,$$

$$\phi_D, \varepsilon_x, \varepsilon_y, \varepsilon_z, \Delta_x, \Delta_y, \Delta_z, \delta b, \delta n]^T \tag{31}$$

where the subscripts N, E, and D represent the north, east, and down local level reference frame, and subscripts x, y, and z the aircraft body reference frame. In Eq. (31) δr_N, δr_E, and δr_D denote the INS position errors; δv_N, δv_E, and δv_D are the INS velocity errors; ϕ_N and ϕ_E are the INS attitude errors; ϕ_D is the azimuth error; ε_x, ε_y, and ε_z are the gyro drifts; Δ_x, Δ_y, and Δ_z are the accelerometer biases; and δb, and δn are the GPS receiver clock drift and clock drift rate. The ε_x, ε_y, and ε_z, Δ_x, Δ_y, and Δ_z, and δn are all modeled as first-order Markov processes. Their correlation time constants are chosen to be 60, 30, and 15 min, respectively. The measurements of the Kalman filter are formed as the differences between the pseudoranges given by the GPS receiver and the line-of-sight (LOS) ranges provided by the INS (see Ref. 11 for more details about the Kalman filter model). The model parameters in the simulations are listed in Table 1. The mission scenario is 4000 s of flight due west at a speed of 300 m/s.

A. Performance of the ARTMAP1

The ARTMAP neural networks are first trained on training databases and then evaluated on testing databases built by Monte-Carlo simulations where different jump-type failures for different sensors are assumed. The values of assumed failures and corresponding input patterns for the ARTb modules are listed in Table 2.

Since the GPS/INS is not completely observable and, hence, cannot reliably distinguish x-gyro failures from y-accelerometer failures (or y-gyro failures from x-accelerometer failures) by using only SCST results, these failures are classified in the same categories in Table 2.

Input patterns for the ARTa are organized from the SCST results of the sensor error states, e.g., ε_x, ε_y, ε_z, Δ_x, Δ_y, Δ_z, δb, and δn at the moment when failures are detected. The method given in the last section is applied to organize input patterns of the ARTMAP1 (the parameter α is chosen as 0.5). As an illustration, the SCST results relevant to the IMU sensor errors for assumed different y-gyro failures are shown in Figs. 4 and 5 (for each of the assumed y-gyro failures, only one curve is shown). Figures 4 and 5 present the SCST results states at the moments when the failures are detected for the training database and the corresponding converted binary patterns, respectively. It is shown that for different y-gyro failures the pattern shapes of the SCST results are very similar (Fig. 4). Hence, it is easy for the ARTMAP1 to reliably recognize failure categories and to determine the specific failure.

The performance of a trained ARTMAP1 network is evaluated by 10 simulation runs for each of the assumed failures. All of the testing results show that the ARTMAP1 system classifies failure positions correctly.

Table 1 Model parameters, 1σ

Error sources	Values
Initial position errors δr_N, δr_W, δr_Z, m	100.0
Initial velocity errors δv_N, δv_W, δv_Z, m/s	1.0
Initial attitude errors Φ_N, Φ_W, arc, s	300.0
Initial azimuth error Φ_Z, arc, s	900.0
Gyro drift Markov processes ε_x, ε_y, ε_z, deg/h	0.05
Gyro white noise, deg/h$^{1/2}$	0.0005
Accelerometer Markov Δ_x, Δ_y, Δ_z, μg	500.0
Accelerometer white noise, $\mu g * s^{1/2}$	1.0
Receiver clock drift δb, m	10.0
Receiver clock drift rate δn, m/s	0.1
Pseudorange white noise, m	5.0

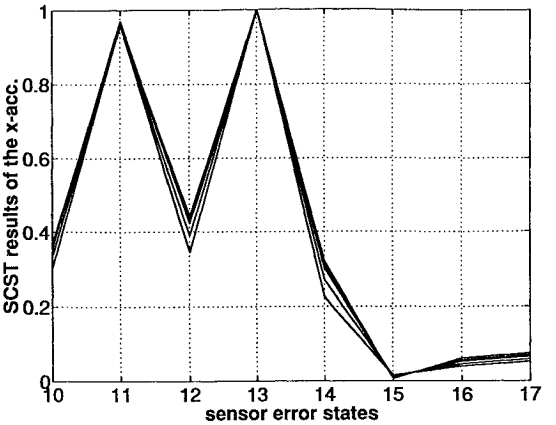

Fig. 4 SCST results of sensor error states when different y-gyro failure are detected.

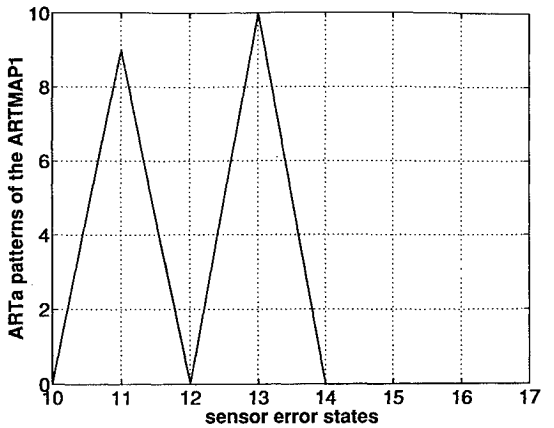

Fig. 5 ARTMAP1 input patterns under different y-gyro failures.

B. Performance of the ARTMAP2

The function of the ARTMAP2 is to determine the time and seriousness of the failure. The ARTMAP2 is first trained on a database formed by simulations with jump-type failures given in Table 2. The ARTa input patterns of the ARTMAP2 are organized using the approach presented in the last section (the sampling window width $L = 60$ s and the integer parameter $h = 10$). Corresponding ARTb input patterns are listed in Table 2. After training, a map is formed from the input patterns of the ARTa into the input patterns of the ARTb. During on-line diagnosis, failure time and failure seriousness are determined by ARTb patterns activated by ARTa input patterns converted from on-line SCST results. The performance of the trained ARTMAP2 network is evaluated on a testing database, where 10 simulation runs are performed for each of the assumed failures with Gaussian noise being added. For the sake of clarity, only simulation results concerned with the y-gyro failures are discussed. Similar results are obtained for the other assumed failures.

Since the SCST results λ_{Δ_x} of the state Δ_x detect the y-gyro failures earlier than others, the ARTMAP2 determines failure time and seriousnesses of the y-gyro failures by analyzing patterns of the

Table 2 Failure assumptions and ARTb patterns

Failure positions	Magnitudes	ARTb patterns ARTMAP1	ARTb patterns ARTMAP2
x accelerometer, μg	600, 700, 800, 900, 1000	1000	1000c[b]
y accelerometer, μg	600, 700, 800, 900, 1000	0100	0100c
x gyro, deg/h	0.5, 1.0, 2.0, 3.0, 5.0	0100	0100c
y gyro, deg/h	0.5, 1.0, 2.0, 3.0, 5.0	1000	1000c
GPS receiver clock, m	50, 70, 100, 150, 200	0010	0010c

[a]Failures occur at $t = 1000$ s. [b]$c = 001, 010, 011, 100, 101$.

Table 3 ARTMAP2 diagnosis results for the y-gyro failures, averaged over 10 runs

Real failure values, deg/h	Diagnosed values, deg/h	Diagnosed failure time, s
0.5	0.6	981
1.0	1.2	986
2.0	2.3	990
3.0	3.1	992
5.0	4.8	993

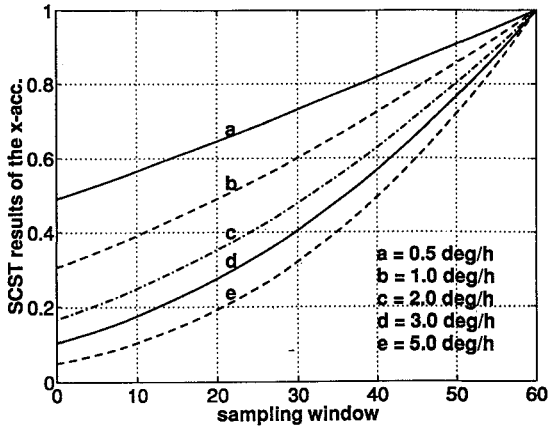

Fig. 6 SCST results of the x-accelerator error state under different y-gyro failures.

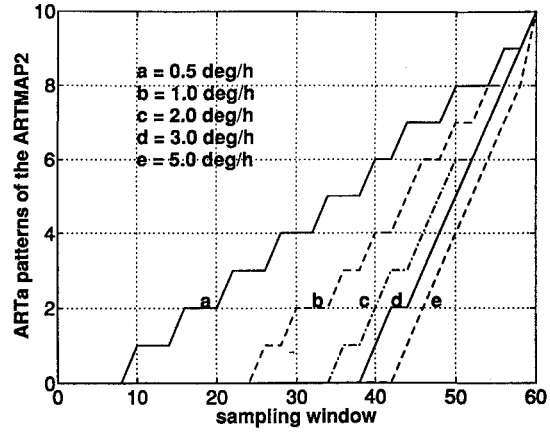

Fig. 7 ARTMAP2 input patterns under different y-gyro failures.

$\lambda_{\Delta_x}(k)$ sampled from time step $k = k_b - L + 1$ to k_b. The $\lambda_{\Delta_x}(k)$ and their corresponding converted patterns of the ARTa for the training database are shown in Figs. 6 and 7. The diagnosis results averaged over 10 runs are presented in Table 3, which shows that despite the influence of noise, the diagnosis results of the ARTMAP2 are quite good. (In our simulations, the diagnosed failure time is always a little ahead of the actual failure time. It is because we use noise-free data to train the network, but we use noisy data to test its performance. System noise will increase the values of the calculated test statistic SCST results.)

Whether we need to use ARTMAP2 to diagnose failure depends on system design requirements. Someone may want to design an integrated GPS/INS that is able to adjust filter parameters adaptively, in order to correct the effects of soft failures. In this case, the ARTMAP2 may be helpful, since it provides the information about the time when the failure happened and also the seriousness of the failure.

V. Isolating Gyro Failures from Accelerometer Failures

Because of the observability problem in GPS/INS systems, a gyro failure may result in residual changes which are very similar to changes resulting from an accelerometer failure and vice versa. Therefore, the SCST results of both state estimates may flag the failure. In such a case, the failure cannot be simply isolated by the ARTMAP1 which locates failures based solely on analyzing the SCST results. In the following, we will show that aircraft maneuvers may be helpful for us to distinguish whether a failure comes from a gyro or an accelerometer, although it may not always be necessary to do so. Our objective here is to present a possible solution for system designers, who try to design a system that can find out exactly where the failures come from, and so that they can use some kind of approach, such as an adaptive filter, to eliminate the effects of soft failures automatically.

For simplicity, the discussion focuses only on the procedure of distinguishing x-accelerometer failures from y-gyro failures. A similar procedure can be applied to distinguish y-accelerometer failures from x-gyro failures. The basic idea of our approach is expressed as follows: After the SCST finds a failure and the ARTMAP1 indicates that the failure comes from either the x accelerometer or the y gyro, let the Kalman filter continuously estimate the error states for a short period of time. No matter which failure has occurred, one of the state estimates, $\hat{\Delta}_x$ or $\hat{\varepsilon}_y$, which corresponds to the failure, is updated correctly, i.e., in the direction of reducing the estimation error, whereas the other state estimate is updated incorrectly, i.e., in the direction of increasing the estimation error. After a short period of time, which of the estimates $\hat{\Delta}_x$ and $\hat{\varepsilon}_y$ is updated correctly can be decided with the help of suitable flight maneuvers. A turn flight maneuver is usually a good choice, because in this situation the system becomes fully observable.[20,21] During flight maneuvers, both estimates $\hat{\Delta}_x$ and $\hat{\varepsilon}_y$ will be updated in the direction of decreasing estimations errors. Hence, the failure position can be easily found by monitoring the change directions of the state estimates and/or their SCST results. The estimate, which is updated following the same direction as that before the maneuver (with its SCST result continuously increasing), corresponds to the actual failure, whereas the other estimate, which is updated toward the opposite direction before the maneuver (with its SCST result droping significantly) does not correspond to the properly working sensor.

A. Simulation Example

The effectiveness of the approach for distinguishing gyro failures from accelerometer failures was examined by simulations where different failures were assumed. Results relative to a ramp-type y-gyro failure are shown in the following. The assumed y-gyro failure $f_{y\text{-gyro}}$ is expressed as

$$f_{y\text{-gyro}} = \begin{cases} 0 & \text{deg/h} \quad 0 \le t \le 1000 \text{ s} \\ \dfrac{t - 1000}{400} & \text{deg/h} \quad 1000 < t \le 1400 \text{ s} \\ 1.0 & \text{deg/h} \quad 1400 < t \le 4000 \text{ s} \end{cases} \tag{32}$$

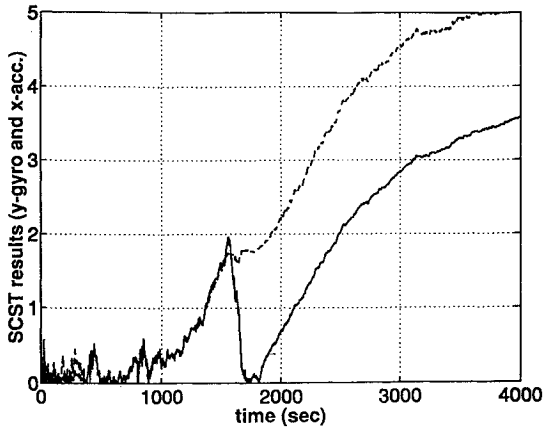

Fig. 8 SCST results of the y-gyro and the x-accelerometer error states under a turn maneuver.

Figure 8 presents the SCST result λ_{Δ_x} (the solid line) of the Δ_x, and λ_{ε_y} (dashed line) of the ε_y. Since the system is not completely observable before the maneuver, the Kalman filter updates both $\hat{\Delta}_x$ and $\hat{\varepsilon}_y$ when the failure occurs. Although $\hat{\varepsilon}_y$ is updated correctly, $\hat{\Delta}_x$ is not. Very similar change processes of λ_{Δ_x} and λ_{ε_y} are observed under the y-gyro failure which is discovered by the SCST at 1350 s. At time 1550 s, a 90-deg left turn is made. During the maneuver, the observability of the GBS/INS is greatly enhanced. Both $\hat{\Delta}_x$ and $\hat{\varepsilon}_y$ are observable. Figure 8 shows that although λ_{ε_y} increases continuously during the maneuver, λ_{Δ_x} drops abruptly because the update of the $\hat{\Delta}_x$ is changed to the opposite direction. Therefore, it can be finally decided that the failure is most likely from the y gyro instead of the x accelerometer.

VI. Conclusions

A systematic scheme for diagnosing failures in dynamic systems is proposed. The concept of using the pattern classification ability of the ARTMAP neural network for failure diagnosis was exploited. In the scheme, two ARTMAP neural networks, ARTMAP1 and ARTMAP2, were applied. Whereas ARTMAP1 finds a failure location by means of recognizing the pattern of the SCST results of sensor errors, at the time when the failure is detected, ARTMAP2 determines when the failure happens and how serious the failure is by analyzing the pattern formed by the time history of the SCST results. The effectiveness of the proposed approach was demonstrated by numerical examples where different failures from gyros, accelerometers, and the GPS receiver in an integrated GPS/INS were successfully diagnosed. An effective approach was also investigated for the purpose of overcoming the difficulty of isolating gyro failures from accelerometer failures. The efficiency of the proposed scheme was demonstrated by a simulation example, where a soft y-gyro failure was correctly located.

Acknowledgment

The authors would like to thank I. Y. Bar-Itzhack of the Technion for his comments and suggestions.

References

[1]Willsky, A. S., "A Survey of Design Methods for Failure Detection in Dynamic Systems," *Automatica*, Vol. 12, 1976, pp. 601–611.

[2]Isermann, R., "Process Fault Detection Based on Modeling and Estimation Methods—a Survey," *Automatica*, Vol. 20, No. 4, 1984, pp. 387–404.

[3]Kerr, T. H., "Decentralized Kalman Filtering and Redundancy Management for Multisensor Navigation," *IEEE Transactions on Aerospace and Electronic Systems*, Vol. 23, No. 1, 1987, pp. 83–119.

[4]Frank, P. M., "Fault Diagnosis in Dynamic System Using Analytical and Knowledge-Based Redundancy—A Survey and Some New Results," *Automatica*, Vol. 26, No. 1, 1990, pp. 459–474.

[5]Gertler, J. J., "Residual Generation," *Control Engineering Practice*, Vol. 1, No. 1, 1993, pp. 3–17.

[6]Patton, R. J., and Chen, J., "Review of Parity Approaches to Fault Diagnosis for Aerospace Systems," *Journal of Guidance, Control, and Dynamics*, Vol. 17, No. 2, 1994, pp. 278–285.

[7]Lin, C. F., *Modern Navigation, Guidance, and Control Processing*, Prentice–Hall Series in Advanced Navigation, Guidance, and Control, and their Applications, Prentice–Hall, Englewood Cliffs, NJ, 1991.

[8]Lin, C. F. (ed.), *Advanced Control System Design*, Prentice–Hall Series in Advanced Navigation, Guidance, and Control, and their Applications, Prentice–Hall, Englewood Cliffs, NJ, 1994.

[9]Brumback, B. D., and Srinath, M. D., "Fault-Tolerant Multisensor Navigation System Design," *IEEE Transactions on Aerospace and Electronic Systems*, Vol. 23, No. 6, 1987, pp. 738–755.

[10]Kerr, T. H., "Real-Time Failure Detection: a Static Nonlinear Optimization Problem that Yields a Two Ellipsoid Overlap Test," *Journal of Optimization Theory and Application*, Vol. 20, No. 4, 1977, pp. 509–536.

[11]Da, R., "Failure Detection of Dynamical Systems with State Chi-Square Test," *Journal of Guidance, Control, and Dynamics*, Vol. 17, No. 2, 1994, pp. 271–277.

[12]Da, R., and Lin, C. F., "An FDI Structure for GPS Autonomous Integrity Monitoring," *Journal of Guidance, Control, and Dynamics* (to be published).

[13]Carpenter, G. A., and Grossberg, S., "A Massively Parallel Architecture for a Self-Organizing Neural Pattern Recognition Machine," *Computer Vision, Graphics, and Image Processing*, Vol. 37, No., 1987, pp. 54–115.

[14]Carpenter, G. A., "Neural Network Models for Pattern Recognition and Associative Memory," *Neural Networks*, Vol. 2, No. 3, 1989, pp. 243–257.

[15]Fukushima, K.,"Neocognition: A Hierarchical Neural Network Capable of Visual Pattern Recognition," *Neural Networks*, Vol. 1, No., 1988, pp. 119–130.

[16]Widrow, B., and Hoff, M. E., "Neural Nets for Adaptive Filtering and Adaptive Pattern Recognition," *Computer*, Vol. 21, No. 1, 1988, pp. 25–39.

[17]Carpenter, G. A., Grossberg, S., and Reynolds, J. H., "ARTMAP: Supervised Real-Time Learning and Classification of Nonstationary Data by a Self-Organizing Neural Network," *Neural Networks*, Vol. 4, No. 5, 1991, pp. 565–588.

[18]Mendenhall, W., and Sincich, T., *Statistics for Engineering and the Sciences*, Dellen, San Francisco, CA, 1992.

[19]Grossberg, S., "Adaptive Pattern Classification and Universal Recoding, I: Parallel Development and Coding of Neural Feature Detectors," *Biological Cybernetics*, Vol. 23, 1976, pp. 121–134.

[20]Goshen-Meskin, D., and Bar-Itzhack, I. Y., "Unified Approach to Inertial Navigation System Error Modeling," *Journal of Guidance, Control, and Dynamics*, Vol. 15, No. 3, 1992, pp. 648–653.

[21]Goshen-Meskin, D., and Bar-Itzhack, I. Y., "Observability Analysis of Piece-wise Constant Systems—Part I: Theory," *IEEE Transactions on Aerospace and Electronic Systems*, Vol. 28, No. 4, 1992, pp. 1056–1067.